Biochimica et Biophysica Acta 1840 (2014) 1135–1144

Contents lists available at ScienceDirect

Biochimica et Biophysica Acta

journal homepage: www.elsevier.com/locate/bbagen

# Powerful tumor cell growth-inhibiting activity of a synthetic derivative of atractyligenin: Involvement of PI3K/Akt pathway and thioredoxin system

Roberta Cotugno [a,1], Dario Gallotta [a,1], Fabrizio Dal Piaz [a], Ivana Apicella [b], Sandro De Falco [b], Sergio Rosselli [c], Maurizio Bruno [c], Maria Antonietta Belisario [a,*]

[a] Department of Pharmacy, University of Salerno, 84084 Fisciano, Salerno, Italy
[b] Angiogenesis Lab, Institute of Genetics and Biophysics "Adriano Buzzati-Traverso" CNR, 80131 Napoli, Italy
[c] Department of Biological, Chemical and Pharmaceutical Sciences and Technologies, University of Palermo, 90128 Palermo, Italy

ARTICLE INFO

*Article history:*
Received 1 August 2013
Received in revised form 31 October 2013
Accepted 27 November 2013
Available online 7 December 2013

*Keywords:*
*Ent*-kaurane
Apoptosis
Cell cycle
PI3K/Akt
Thioredoxin system
HCT 116 xenograft

ABSTRACT

*Background:* The semi-synthetic *ent*-kaurane 15-ketoatractyligenin methyl ester (SC2017) has been previously reported to possess high antiproliferative activity against several solid tumor-derived cell lines. Our study was aimed at investigating SC2017 tumor growth-inhibiting activity and the underlying mechanisms in Jurkat cells (T-cell leukemia) and xenograft tumor models.
*Methods:* Cell viability was evaluated by MTT assay. Cell cycle progression, reactive oxygen species (ROS) elevation and apoptotic hallmarks were monitored by flow cytometry. Inhibition of thioredoxin reductase (TrxR) by biochemical assays. Levels and/or activation status of signaling proteins were assessed by western blotting. Xenograft tumors were generated with HCT 116 colon carcinoma cells.
*Results:* SC2017 displayed cell growth-inhibiting activity against Jurkat cells (half maximal inhibitory concentration values (IC50) < 2 μM), but low cell-killing potential in human peripheral blood mononuclear cells (PBMC). The primary response of Jurkat cells to SC2017 was an arrest in $G_2$ phase followed by caspase-dependent apoptosis. Inhibition of PI3K/Akt pathway and TrxR activity by SC2017 was demonstrated by biochemical and pharmacological approaches. At least, SC2017 was found to inhibit xenograft tumor growth.
*Conclusions:* Our results demonstrate that SC2017 inhibits tumor cell growth in *in vitro* and *in vivo* models, but displays moderate toxicity against PBMC. We also demonstrate that SC2017 promotes caspase-dependent apoptosis in Jurkat cells by affecting Akt activation status and TrxR functionality.
*General significance:* Our observations suggest the semi-synthetic *ent*-kaurane SC2017 as a promising chemotherapeutic compound. SC2017 has, indeed, shown to possess tumor growth inhibiting activity and be able to counteract PI3K/Akt and Trx system survival signaling.



## 1. Introduction

*Ent*-kauranes are an important class of tetracyclic diterpenoids constituted by a perhydrophenantrene unit fused with a cyclopentane unit forming a bridge between carbons C-8 and C-13 [1]. *Ent*-kaurane diterpenes are present in different plant species belonging to several families such as Asteraceae, Euphorbiaceae, Apiaceae, Lamiaceae and other families [1] and have been shown to possess several biological activities [2–4], including pro-apoptotic [5] anti-inflammatory [6], antibacterial [7] and anti-HIV [8].

The main structural determinant for cytotoxicity of *ent*-kaurane compounds has been shown to be the α,β-unsaturated group [9,10], even if the selectivity and the potency of different compounds depend on the other functional groups present into the *ent*-kaurane skeleton. One of the more interesting *ent*-kauranes containing an α,β-unsaturated group is oridonin isolated from *Isodon rubescens*. The antitumor potential of oridonin has been, indeed, highlighted in a huge number of studies in *in vitro* as well *in vivo* experimental models [11,12].

In view of the potential use of this class of diterpenes as drug or lead compounds, synthetic derivatives of atractyligenin, the nor-*ent*-kaurane diterpene aglycon of the glycoside atractyloside (atractyligenin), which occurs in *Atractylis gummifera* L. (Asteraceae), were obtained by including α,β-unsaturated ketone moiety [13]. Among these, the 15-ketoatractyligenin methyl ester, here named SC2017, showed high antiproliferative activity in several solid-tumor cell lines [13].

Here we demonstrate that SC2017 possesses powerful cell growth-inhibiting activity, even higher than that of oridonin, in leukemia-

* Corresponding author at: Department of Pharmacy, University of Salerno, Via Giovanni Paolo II 132, 84084 Fisciano, Salerno, Italy. Tel.: +39 089 969740; fax: +39 089 969602.
*E-mail address:* mabelisario@unisa.it (M.A. Belisario).
[1] Equal contributing authors.

0304-4165/$ – see front matter © 2013 Elsevier B.V. All rights reserved.
http://dx.doi.org/10.1016/j.bbagen.2013.11.023

derived cell lines, but low cytotoxicity in peripheral blood mononuclear cells (PBMC) from healthy donors. SC2017 antiproliferative potential was analyzed in detail in Jurkat cells, showing involvement of cell cycle progression impairment and induction of caspase-dependent apoptosis. The purpose of the present study was also to explore the mechanism(s) underlying the cell growth-inhibiting activity of SC2017. By biochemical and pharmacological approaches, we demonstrated the ability of SC2017 to affect PI3K/Akt pathway and the thioredoxin (Trx) system, two key players of tumor cell survival machinery [14,15]. Inappropriate activation of PI3K/Akt pathway and higher expression of Trx and its reductase (TrxR) in cancers are well documented [16,17]. The SC2017 anti-tumor potential was also evaluated in HCT 116 xenograft tumors.

## 2. Materials and methods

### 2.1. Reagents and antibodies

Fetal bovine serum (FBS) was from GIBCO (Life Technologies, Grand Island, NY, USA). Hoechst 33342 and LY294002 were from Invitrogen (Life Technologies, Grand Island, NY, USA), Z-VAD-fmk (ZVAD) was from BD Pharmigen (Franklin Lakes, NJ, USA), MK-2206 (S1078) from Selleckchem (Houston, TX, USA), and thioredoxin reductase (TrxR) from rat liver and all the other reagents, unless otherwise specified, were from Sigma-Aldrich (St. Louis, MO, USA). The antibodies anti-Hsp60 (mouse monoclonal, sc-13115), anti-GAPDH (mouse monoclonal, sc-32233), anti-Cdc2 (mouse monoclonal, sc-8395), anti-phospho (Thr161)-Cdc2 p34 (rabbit polyclonal, sc-101654), anti-α tubulin (mouse monoclonal, sc-32293), anti-cytochrome *c* (rabbit polyclonal, sc-7159), anti-PARP-1 (mouse monoclonal, sc-8007), and anti-Bcl-2 (C-2, mouse monoclonal, sc-7382) were obtained from Santa Cruz Biotechnology (Santa Cruz, CA, USA). Anti-pAkt (Ser 473, mouse mAb, 9271), anti-Akt (rabbit polyclonal, 9272), anti-cleaved caspase 3 (Asp 175, rabbit polyclonal, 9661), and anti-cyclin B1 (mouse monoclonal, 4135) were from Cell Signaling Technology (Danvers, MA, USA); appropriate peroxidase-conjugated secondary antibodies were from Jackson ImmunoResearch (Baltimore, PA, USA).

SC2017 (Fig. 1) was synthesized and identified as previously reported [13]. SC2017 stock solutions (181 mM) in DMSO were aliquoted and stored in the dark at 4 °C.

### 2.2. Cells and treatments

Jurkat and U937 cells, obtained from Cell Bank in GMP-IST (Genova, Italy), were maintained in RPMI 1640 medium, 2 mM L-glutamine and antibiotics at 37 °C in humidified atmosphere with 5% $CO_2$. HCT 116 and MCF7 cells were obtained from American Type Culture Collection (ATCC) (Manassas, VA, USA). HCT 116 were maintained in McCoy's 5a medium supplemented with 4 μg/ml of transferrin, 5 μg/ml of insulin, and 10 ng/ml of EGF. MCF7 was maintained in Dulbecco's modified eagle's medium (DMEM). All media were supplemented with 10% (v/v) FBS. To ensure logarithmic growth, cells were sub-cultured every two days. Under given experimental conditions, control cells were able to double their number within 24 h.

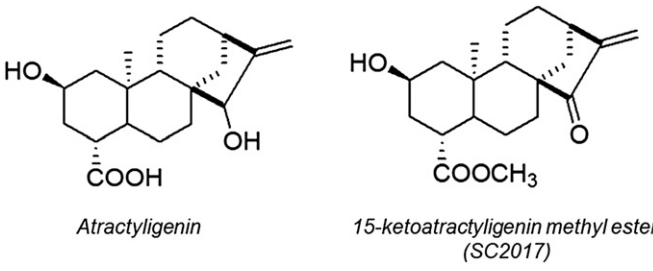


**Fig. 1.** Structure of atractyligenin and its derivative 15-ketoatractyligenin methyl ester (SC2017).

Human peripheral blood mononuclear cells (PBMC) were isolated from buffy coats of healthy donors (kindly provided by the Blood Center of the Hospital of Battipaglia, Salerno, Italy) by using a standard Ficoll–Hypaque gradient. Freshly isolated PBMC contained 90.6 ± 1.2% live cells as assessed by the manual Trypan blue exclusion method. Resting PBMC and PBMC induced to proliferate by phytohemagglutinin (PHA) (10 μg/ml) were used to evaluate SC2017 cytotoxic and cytostatic effects, respectively.

SC2017 working solutions were prepared in culture medium immediately prior to use; the final concentration of DMSO, never exceeding 0.15% (v/v), was equal in samples and controls.

### 2.3. Analysis of cell proliferation and viability

Cells were seeded in 96-well plates and incubated for the established times in the absence and in the presence of different concentrations of SC2017. Jurkat and U937 cells were seeded at a cell density of $2 \times 10^4$/well; HCT 116 and MCF7 were seeded at a density of $1.5 \times 10^4$/well the day before treatment. The number of viable cells was quantified by MTT ([3-(4,5-dimethylthiazol-2-yl)-2,5-diphenyl tetrazolium bromide]) assay. Absorption at 550 nm for each well was assessed using a microplate reader (LabSystems, Vienna, VA, USA). To exclude any interference of SC2017 with the tetrazolium salt-based assay, cell growth inhibition was randomly verified also by cytometric count (Trypan blue exclusion test). IC50 values were calculated from cell viability dose–response curves and defined as the concentration resulting in 50% inhibition in cell survival as compared to controls.

### 2.4. Flow cytometry analysis

Flow cytometry analysis was performed using a BD FACSCalibur™ instrument (Becton Dickinson, San Jose, CA, USA). Cellular DNA content was evaluated by propidium iodide (PI) staining of permeabilized cells according to the available protocol [18]. Data from 10,000 events per sample were collected. The percentages of the elements in the hypodiploid region and in $G_0/G_1$, S, and $G_2$/M phases of the cell cycle were calculated using the CellQuest or MODFIT software, respectively. The percentages of cells actively undergoing apoptosis was determined by a Human Annexin V/FITC kit (Bender MedSystems, Vienna, Austria) according to the manufacturer's instructions. Green (Annexin V-FITC) and red (PI) fluorescence of individual cells were measured. Electronic compensation was required to exclude overlapping of the two emission spectra. Changes of mitochondrial membrane potential were monitored (FL-2 channel) using the mitochondrial membrane potential-driven uptake of fluorescent tetramethylrhodamine ethyl ester (TMRE) (5 nM, final concentration). The intracellular levels of reactive oxygen species (ROS) were measured by 2′,7′-dichlorodihydrofluorescein diacetate (DCFHDA) as previously described [19]. t-Butylhydroperoxide (t-BOOH, 300 μM) was included as a positive control.

### 2.5. Microscopic analysis

Hoechst 33342 (10 μg/ml) staining was used for apoptotic nuclei determination. Cells were analyzed by the Zeiss Axiovert 200 microscope with a 40× objective ($\lambda_{exc}$, 351 nm; $\lambda_{em}$, 380 nm) and images were acquired from randomly selected fields.

### 2.6. Western blot analysis

Whole lysates for immunoblot analysis were prepared according to standard protocols. Cytosolic protein extracts for determining cytochrome *c* were prepared as described previously [18]. Clarified whole lysate and cytosolic proteins were fractionated on SDS-PAGE (20–50 μg/lane) under reducing conditions. Protein concentration in

samples was determined by DC Protein Assay (Bio-Rad, Berkeley, CA, USA). The percentage of polyacrylamide was chosen on the basis of the MW of the protein to detect. Proteins were transferred onto nitrocellulose membranes and immunoblotted with the appropriate primary antibodies. Signals were visualized with the appropriate horseradish peroxidase-conjugated secondary antibodies and enhanced chemiluminescence (Amersham Biosciences-GE Healthcare, NY, USA). Densitometry of bands was performed with NIH ImageJ software.

### 2.7. Thioredoxin reductase activity

#### 2.7.1. Cell-free system

TrxR (1 μM) was pre-reduced by incubation for 5 min at room temperature (r.t.) with 0.1 mM NADPH in 100 mM Hepes buffer (pH 7.2), containing 5 mM EDTA. Different doses of SC2017 or vehicle were then added to the mixture. After 30 min at r.t., pre-incubation mixtures were added to Hepes buffer containing 0.1 mM NADPH and 2 mM 5,5′-dithiobis(2-nitrobenzoic acid) (DTNB). The increase in absorbance at 412 nm was recorded against a blank containing all the reagents except TrxR. In preliminary experiments, possible artifacts due to the formation of a colorless SC2017–TNB complex were excluded by adding SC2017 6 min after starting TrxR-mediated TNB formation and reading the absorbance at 412 nm.

#### 2.7.2. Cell lysate

Control cells or cells exposed to 20 μM SC2017 were incubated for 90 min and then lysed by sonication in PBS containing the protease inhibitor cocktail (Sigma, P2714). The activity of TrxR was measured in 96-well plates. Cell extracts (50 μg) were incubated with 100 mM Hepes buffer (pH 7.2), containing 1 mM EDTA, 1 mM NADPH and 2 mM DTNB. After 10 min at r.t., the reactions were stopped by the addition of 6 M guanidine-HCl and the absorbance at 412 nm was recorded by using a microplate reader (LabSystems, Vienna, VA, USA). Values were subtracted for the absorbance of a blank containing all the reagents except NADPH. In addition, blanks containing DTNB alone or plus NADPH were included in the experiments.

### 2.8. Xenograft tumor

For xenograft tumor experiments, $5 \times 10^6$ HCT 116 human colon carcinoma cells were injected subcutaneously in 20 8-week-old CD1 nude athymic mice. After 7 days, when tumors reached a volume between 50 and 100 $mm^3$, animals were divided into two groups ($n = 8$) and treated with SC2017 at 10 mg/kg or vehicle. SC2017 was dissolved in the adjuvant composed by PEG400/sterile water 1:1 at the concentration of 2.5 mg/ml, and 100 μl were delivered daily by intraperitoneal injection. Tumor growth was followed by three weekly measurements of tumor diameters with a caliper. Tumor volume (TV) was calculated according to the formula: $TV\ (mm^3) = d^2 \times D / 2$, where d and D are the shortest and the longest diameters, respectively. For ethical reasons, mice were sacrificed when control tumors reached in average a volume of 1500 $mm^3$, that occurred after 14 days of treatment. For animal experiments, the care and husbandry of mice and tumor experimental procedures were in accordance with European Directive 86/609 and with Italian Decreto Legge (D.L.) 116. All experiments were approved by the Institute of Genetics and Biophysics veterinarian.

### 2.9. Statistical analysis

#### 2.9.1. In vitro assay

Unless otherwise specified data reported in each figure are the mean value ± SEM of at least three experiments performed in duplicate. Differences between treatment groups were analyzed by the student *t* test and were considered significant when $p < 0.05$.

#### 2.9.2. In vivo assay

Data are expressed as mean ± SEM, with $p < 0.05$ considered statistically significant. Differences among groups were tested by one-way ANOVA. Tukey HD test was used as post hoc test to identify which group differences account for the significant overall ANOVA. All calculations were carried out using SPSS statistical package (vers12.1, Chicago, IL).

## 3. Results

### 3.1. SC2017 strongly reduces human cancer cell growth

Exponentially growing cultures of Jurkat (T-cell leukemia), U937 (monocytic leukemia), MCF7 (breast carcinoma) and HCT 116 (colon carcinoma) cells were exposed to increasing concentrations of SC2017 and cell viability was evaluated at 24 h by MTT assay. For comparison, half maximal inhibitory concentration (IC50) values were calculated on dose–response curves (Table 1). SC2017 displayed the strongest cell growth-inhibiting activity in both leukemia-derived cell lines as indicated by the lower than 4 μM IC50 values. Jurkat cells were about two fold more susceptible than U937 cells. MCF7 cells were included in the experimentation for comparison with data previously reported by Rosselli et al. [13] on the antiproliferative potential of SC2017. The differences between our and their IC50 values (about 7.5 μM and 2 μM, respectively) are presumably because they measured the antiproliferative potential of SC2017 at 72 h instead of 24 h. Indeed, the antiproliferative effect of SC2017 increased in function of incubation time, resulting in the IC50 values being more than halved at 48 h in all cell types (data not shown). HCT 116 cells were included because these were subsequently used for an *in vivo* xenograft study (Section 2.8). Remarkably, under our experimental conditions and in agreement with previous reports [12], we found that oridonin, a natural diterpene lactone widely known for its antitumor potential [11,12], exhibited lower antiproliferative activity against all tested cell lines than SC2017 (Table 1).

We chose to further characterize the mechanism(s) underlying the SC2017 antiproliferative effect in Jurkat cells, due to the high susceptibility to the chemical of this cell line.

### 3.2. SC2017 inhibits cell proliferation by inducing apoptosis and cell cycle arrest

We investigated whether SC2017 reduced Jurkat cell number by affecting cell cycle progression and/or by inducing cell death. Cells were exposed for 24 h to 1.5 μM and 2.5 μM, two doses close to SC2017 IC50 value in this cell line and DNA content was evaluated by flow cytometry analysis of propidium iodide (PI) stained nuclei. Data in Fig. 2A show that SC2017 caused cells to accumulate in $G_2$/M and, less markedly, in S. A shift of cell cycle profile towards the left can be observed at 2.5 μM SC2017. This shift can be ascribed to a concomitant increase of cells with a DNA content lower than $G_0/G_1$ ($subG_0/G_1$), a hallmark of apoptotic death. In fact, apoptotic DNA fragmentation occurring in $G_2$/M (4n) arrested cells may lead to a "$subG_2$/M" cell

**Table 1**
Comparison of tumor cell growth inhibition activity of SC2017 and oridonin.

| Cell lines | IC50 (μM)[a] | |
|---|---|---|
| | SC2017 | Oridonin |
| Jurkat | 1.68 ± 0.11[b] | 5.4 ± 0.48 |
| U937 | 3.2 ± 0.28 | 11.2 ± 0.81 |
| HCT 116 | 5.8 ± 0.49 | 16.8 ± 1.62 |
| MCF7 | 7.4 ± 0.82 | 29.1 ± 2.31 |

[a] The concentration resulting in 50% inhibition in cell survival as compared to controls.
[b] Mean values ± SEM from three experiments done in quadruplicate.

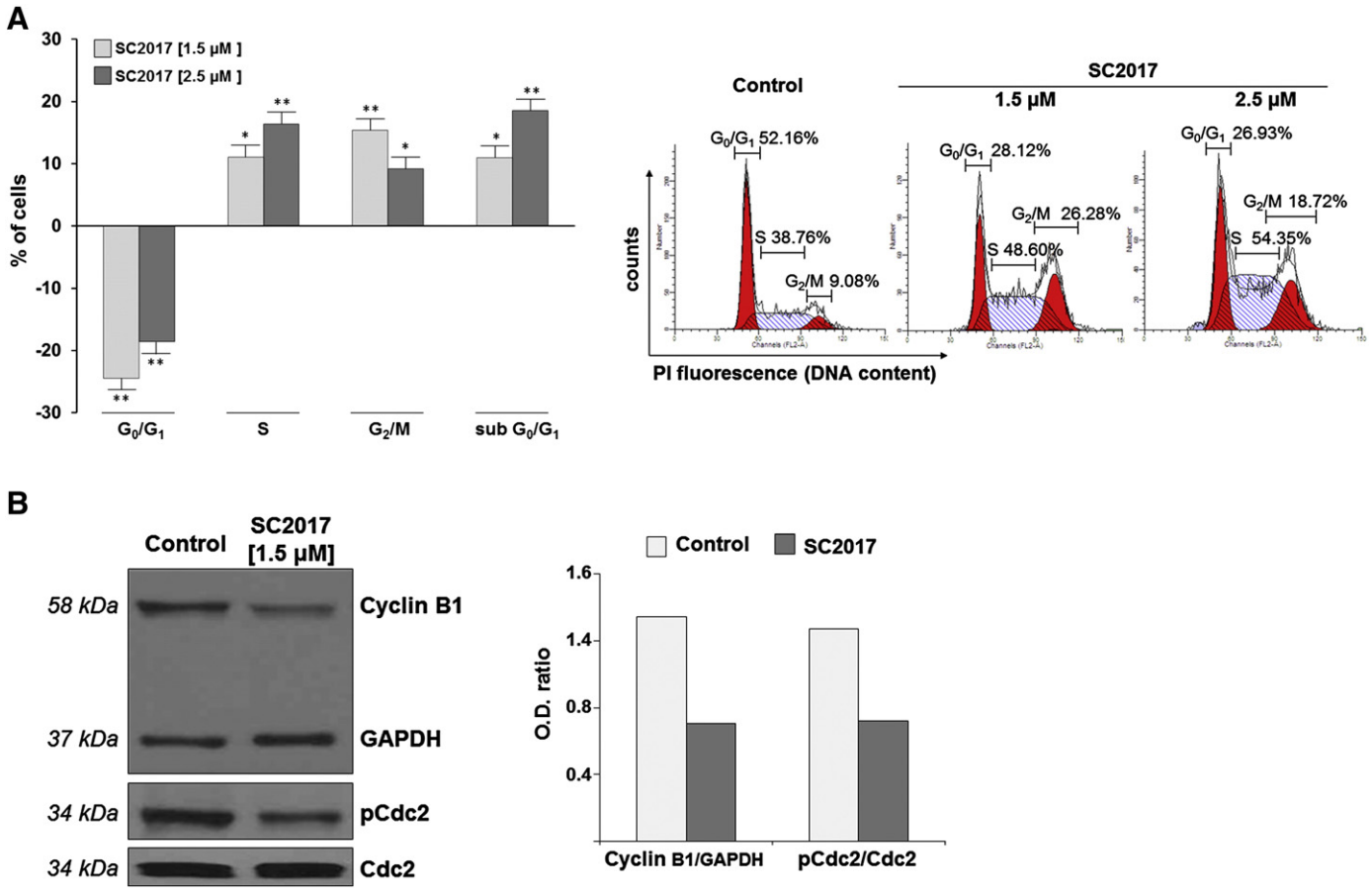


**Fig. 2.** Effect of SC2017 on cell cycle progression and DNA fragmentation. (A) Flow cytometric evaluation of DNA content in Jurkat cells exposed for 24 h to SC2017 or vehicle alone (control). Data are presented as the increase/decrease of the percentages of treated cells with a specific DNA content with respect to the corresponding percentages in control cells (values in control cells: sub$G_0/G_1 \leq 2\%$; $G_0/G_1$, 55.43 ± 2.2%; S, 36.58 ± 2.3%; $G_2/M$, 7.99 ± 1.2%). Representative histograms are shown on the right. Data reported are mean values ± SEM from three experiments done in duplicate (*$p < 0.05$, **$p < 0.001$, raw data of samples *vs* control cells). (B) Cyclin B1, Cdc2 and pCdc2 (Thr161) levels in control and SC2017-treated cell lysates. GAPDH was included as a loading control. Densitometry of bands is shown on the right. Blots are representative of at least two separate experiments with similar results.

population, which is artefactually integrated as "S phase" and so on [20]. Cells exposed to 2.5 μM SC2017 for 16–18 h displayed, indeed, lower percentages of hypodiploid cells, but a more marked $G_2/M$ arrest than at 24 h (data not shown).

Since flow cytometric analysis of DNA content does not allow to discriminate between $G_2$ (4n) and M (4n) arrest, we evaluated the levels of cyclin B1 and pCdc2 (Thr161), key regulators of M phase entry, in cells exposed to SC2017. Blots in Fig. 2B show that 1.5 μM SC2017-treated cells displayed reduced levels of both cyclin B1 and pCdc2, thus indicating that cells were arrested in $G_2$ phase.

Cell population integrated as sub$G_0/G_1$ may include also necrotic cells, thus we took advantage of Annexin V/PI test to conclusively assess whether SC2017 induced cell death by apoptosis. This test allowed us to simultaneously monitor PS exposure, a hallmark of apoptosis (cells positive for Annexin V staining, $A^+$), and plasma membrane damage occurring in "late" apoptosis or necrosis (cells positive for PI staining, $PI^+$). As summarized in Fig. 3A, SC2017 caused a dose-dependent increase of early and late apoptotic cells, without activating, at least up to 2.5 μM, necrotic processes. Microscopic analysis of DAPI-stained nuclei showed an increase of cells displaying typical features of apoptosis, such as condensed chromatin and nuclear fragmentation (Fig. 3B), thus confirming SC2017-induced apoptotic mode of cell death.

### 3.3. SC2017 induces mitochondrial dysfunction and cytochrome c release

Involvement of mitochondria in SC2017-induced apoptosis was evaluated by monitoring changes of the electrochemical gradient ($\Delta\Psi m$) by flow cytometry. Cytograms in Fig. 4A (left panel) show that SC2017 induced a marked and dose-dependent reduction of mitochondrial membrane potential. Moreover, by monitoring the kinetics of SC2017-promoted mitochondrial depolarization and PS exposure, we found that $\Delta\Psi m$ dissipation occurred earlier than Annexin V positivity ($A^+$ cells = $A^+/PI^-$ plus $A^+/PI^+$ cells) (Fig. 4A, right panel).

The cytosolic release of pro-apoptotic proteins, such as cytochrome *c*, is a key event in the mitochondrial-dependent apoptotic death process [21]. Accordingly, to a primary role of mitochondria in SC2017-triggered apoptosis, leakage of cytochrome *c* was detectable as early as 14 h following Jurkat cell exposure to SC2017 (Fig. 4B).

Bcl-2 is known to be a potent inhibitor of mitochondrial-dependent apoptosis in response to a variety of cytotoxic agents by preventing disruption of the outer mitochondrial membrane [22]. However, we found that the levels of Bcl-2 protein remained unchanged following Jurkat cell incubation for 12 h and 18 h with SC2017 (Fig. 4B).

Next we evaluated whether reactive oxygen species (ROS) generation was rather the primary cause of SC2017-induced $\Delta\Psi m$ loss. The levels of ROS were monitored at 1 h, 2 h, 5 h, and 10 h following SC2017 cell treatment, that is before the onset of extensive mitochondrial membrane depolarization. In fact, intracellular ROS elevation may be a cause and/or a consequence of mitochondrial dysfunction [23]. Flow cytometry analysis of DCFHDA-loaded cells showed that SC2017 at all tested concentrations, except 5 μM, failed to increase the basal ROS levels in Jurkat cells (Supplementary Fig. 1). However, also at 5 μM, a strongly cytotoxic dose, SC2017 treatment caused only a 3-

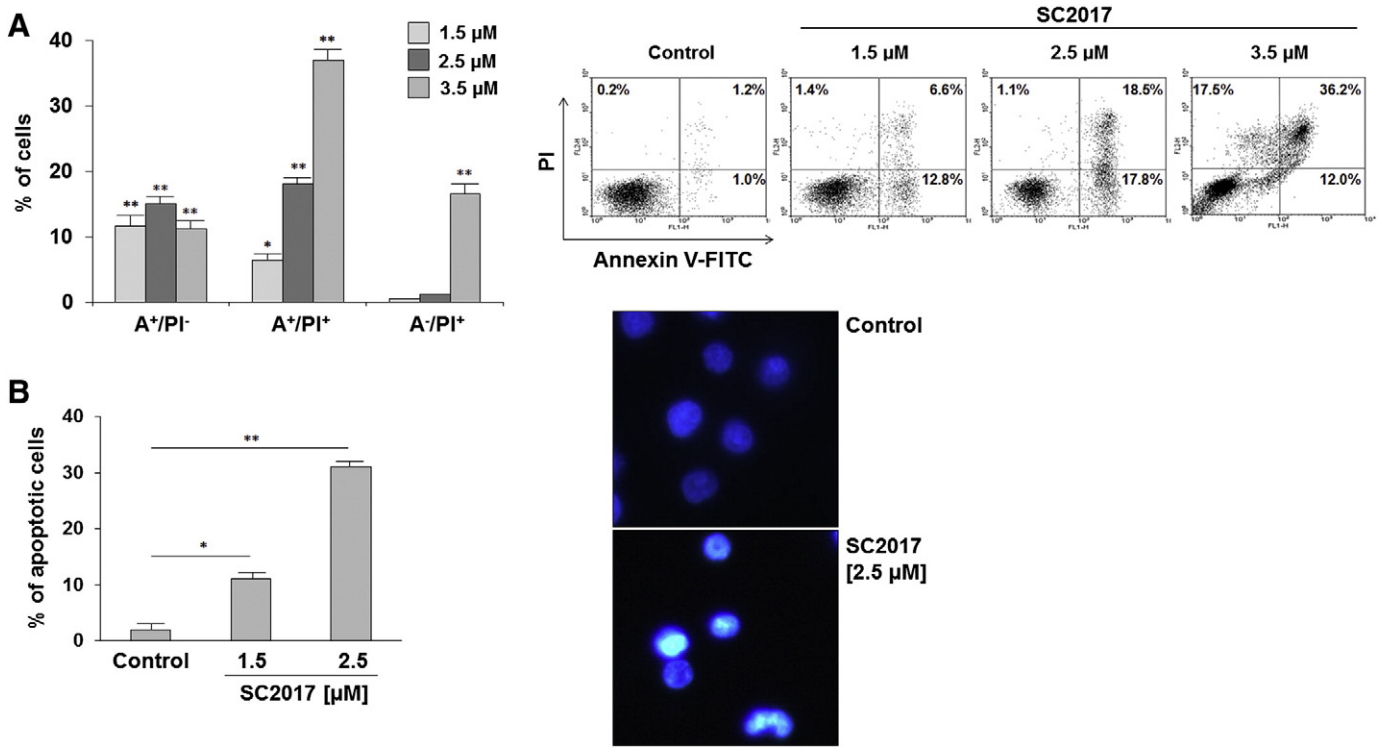


**Fig. 3.** SC2017 induces apoptosis in Jurkat cells. (A) Jurkat cells, exposed for 24 h to increasing doses of SC2017 or vehicle alone (control), were double stained with Annexin V-FITC and PI and analyzed by flow cytometry. $A^-/PI^-$, viable cells; $A^+/PI^-$, early apoptotic cells; $A^+/PI^+$, late apoptotic cells; $A^-/PI^+$, necrotic cells. On the Y axis, the percentages of SC2017-treated Jurkat cells in each quadrant subtracted for the percentage of control cells in the same quadrant (vehicle only: ≤2.0% in all quadrants); *p < 0.05, **p < 0.001, raw data of samples *vs* controls. Representative cytograms are on the right. (B) Quantitative evaluation of cells displaying apoptotic features after exposure to increasing SC2017 doses for 24 h (percentages of 100 nuclei examined). Data are mean values ± SEM from at least two experiments done in duplicate (*p < 0.05, **p < 0.001 *vs* controls). On the right, fluorescence microscopy images of Hoechst-stained nuclei of control and 2.5 μM SC2017-treated cells.

fold increase of control cell DCF mean fluorescence *versus* an increase of more than 10-fold induced by t-BOOH, used as a positive control.

### 3.4. SC2017 induces caspase-dependent apoptosis

Caspase 3 activation was evaluated in Jurkat cells exposed to 2.5 μM SC2017 by western blotting. The blots in Fig. 5A clearly show the presence of caspase 3 proteolytic fragments and cleaved poly ADP-ribose polymerase (PARP-1), one of the caspase 3 substrates. Cell pretreatment with ZVAD, a pan-caspase inhibitor, prevented both caspase 3 proteolytic activation and PARP-1 digestion.

The contribution of caspase pathways to SC2017-mediated apoptotic cell death was assessed also by monitoring the effect of ZVAD on the extent of SC2017-induced ΔΨm loss and PS exposure. Caspase pathway inhibition by ZVAD caused a more than 3-fold reduction of both early and late apoptotic cell populations in SC2017-treated Jurkat cells (Fig. 5B); however a concomitant switch *versus* necrotic mode of cell death was observed. Pre-treatment of cells with ZVAD also reduced the extent of mitochondrial potential dissipation, but less efficiently than PS exposure. The lower efficiency of ZVAD in preventing mitochondrial damage was still more marked at incubation times shorter than 24 h (data not shown).

### 3.5. Role of PI3K/Akt pathways in SC2017-induced apoptosis in Jurkat cells

Akt, the major downstream effectors of PI3K survival signals, is known to inhibit the release of cytochrome *c* induced by pro-apoptotic agents [24,25]. Thus we examined the effect of SC2017 on Akt constitutive phosphorylation at Ser473 (pAkt) in Jurkat cells [26]. Blots in Fig. 6A show that SC2017 prevented Akt phosphorylation in a time- and dose-dependent manner. At 14 h incubation with 2.5 μM and 1.5 μM Akt constitutive phosphorylation was reduced by about 66% and 42%, respectively. No changes of Akt protein levels were instead observed.

Next, we evaluated the effect of PI3K pharmacological inhibition on the extent of SC2017-triggered apoptosis. Jurkat cells were exposed for 2 h to 15 μM LY294002, an inhibitor of PI3K, or to 1 μM MK-2206, an Akt allosteric inhibitor. The concentration of the two inhibitors was chosen on grounds of earlier publications [19,27] to obtain Akt phosphorylation inhibition without extensive toxicity. Cells were then incubated for further 24 h with 1.5 μM SC2017, a dose at which the drug elicited mainly a cytostatic response and low apoptosis (see Fig. 3A). Data in Fig. 6B show that both the inhibitors potentiate the apoptotic response of Jurkat cells to SC2017. However, while MK-2206 causes a substantially additive effect, LY294002 strongly enhances the pro-apoptotic potential of SC2017 causing a more than 3-fold increase of the percentage of apoptotic Annexin V-positive cells. Similarly, the combined treatment with LY294002 caused a more marked increase of cells with depolarized mitochondria compared to MK-2206 (data not shown).

### 3.6. SC2017 inhibits the thioredoxin system

The presence of functional thiols in Trx and TrxR makes these proteins suitable targets for SC2017 α,β-unsaturated carbonyl. Here, we focused on SC2017 ability to inhibit TrxR activity, because the mammalian reductase contains, in addition to the catalytic cysteine (Cys) in the active site, also a high reactive and easily accessible selenocysteine (Sec), essential for its redox activity [28,29]. Firstly, we demonstrated the ability of SC2017 to inhibit TrxR activity in a cell-free system using DTNB as synthetic substrate and NADPH as an electron donor (Fig. 7A). Next, the effect of SC2017 on cellular TrxR was evaluated by incubating Jurkat cells with 20–75 μM SC2017 for 90 min. Such experimental conditions were chosen because preliminary wash-out experiments indicated that the use of high doses of the drug, but at a short incubation time,

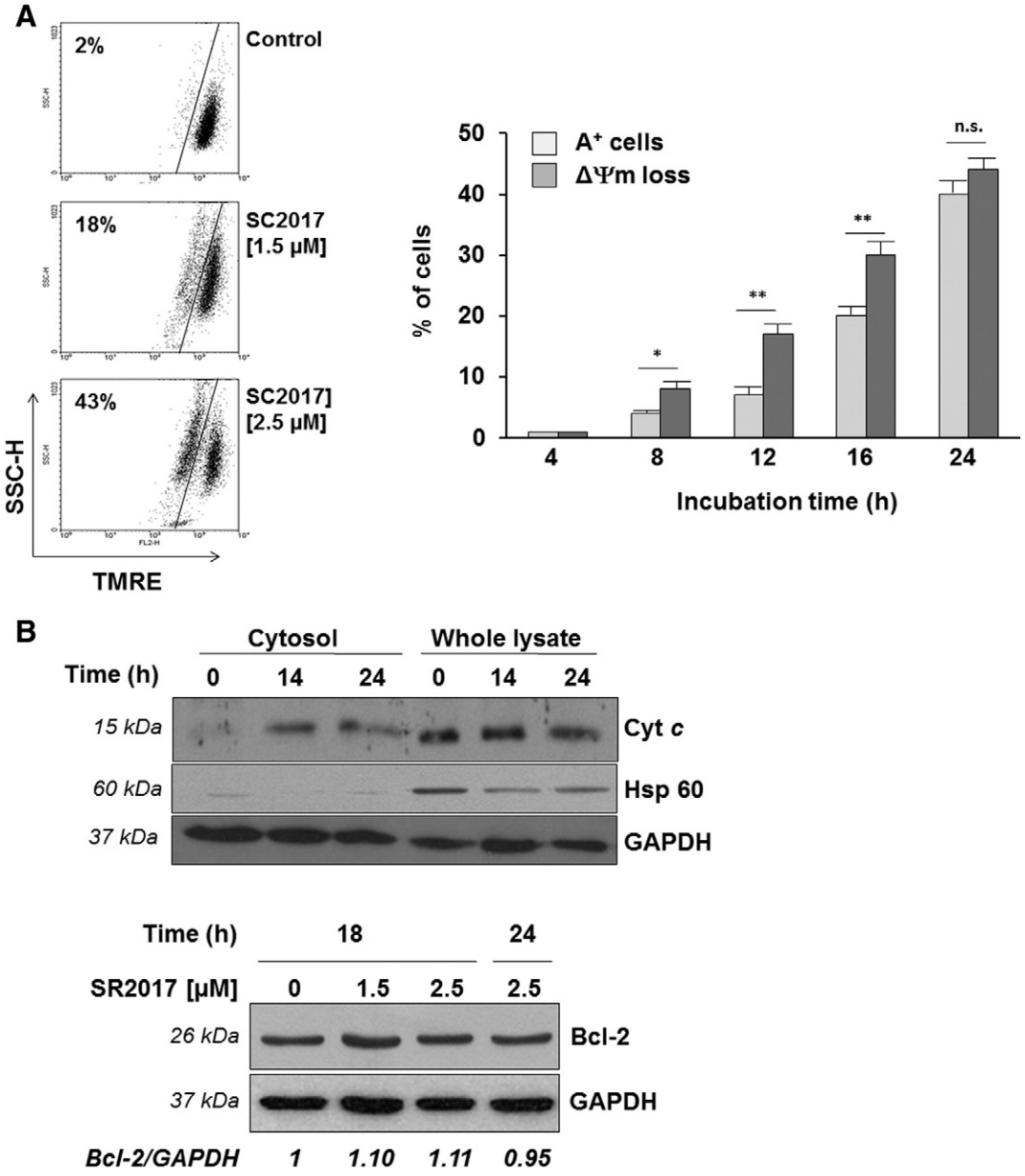


**Fig. 4.** Effect of SC2017 on mitochondrial membrane potential, cytochrome *c* release and Bcl-2 protein levels. (A) Left panel: mitochondrial potential dissipation in Jurkat cells exposed to SC2017 for 24 h. Control cells treated with the vehicle only were incubated for the same time. Cytograms are representative of at least three separate experiments with comparable results. Right panel: comparison of phosphatidylserine exposure ($A^+$ cells) and ΔΨm loss kinetics in Jurkat cells exposed to 2.5 μM SC2017; on the Y axis, the percentages of cells in a gated region subtracted for the percentage of control cells in that region; data are mean values ± SEM from at least two experiments done in duplicate (*$p < 0.05$, **$p < 0.001$, n.s. not significant, raw data of samples *vs* controls). (B) Upper blots: cytosolic fractions (40 μg) and whole lysates (20 μg) from Jurkat cells exposed for the indicated times to 2.5 μM SC2017, were probed with anti-cytochrome *c* antibody and reprobed with anti-Hsp60 to check the purity of the cytosolic fractions. GAPDH was included as loading control. Lower blots: total Bcl-2 levels in Jurkat cells following exposure to SC2017. GAPDH was included as a loading control. Densitometry of bands is indicated: Bcl-2/GAPDH is the ratio of Bcl-2 to GAPDH normalized to the control (time 0). Blots are representative of at least two experiments with similar results.

allowed the chemical to enter without causing extensive cell death (data not shown). At the end of incubation, TrxR activity was measured by following DTNB reduction. Data summarized in Fig. 7B clearly show that SC2017 inhibited TrxR activity in a dose-dependent fashion.

### 3.7. Cytotoxic/cytostatic SC2017 potential in PBMC

The cytotoxic potential of SC2017 was evaluated in PBMC from healthy donors, chosen as the normal counterpart of leukemia-derived Jurkat cell line. SC2017 did not cause any significant reduction of the number of freshly isolated non-proliferating PBMC, at least in the range of doses cytotoxic in leukemia cells (Fig. 8A). We monitored also the effect of SC2017 on cell cycle progression of PHA-stimulated PBMC. Mitogen-treated PBMC were exposed to 5 μM SC2017 (a dose highly cytotoxic in Jurkat cells, but not in PBMC) or vehicle only, and the distribution of cells in the different phases of a cell cycle after 72 h incubation was monitored by flow cytometry. Data summarized in Fig. 8B show that while cell cycle progression of control PBMC was clearly apparent, most, if not all, of the SC2017-treated PBMC remained accumulated in $G_0/G_1$ phase. It should be underlined that in both control and SC2017-treated PBMC about 20% of the cell population underwent necrosis during the experimentation, as inferred by PI staining under non-permeabilizing conditions (data not shown).

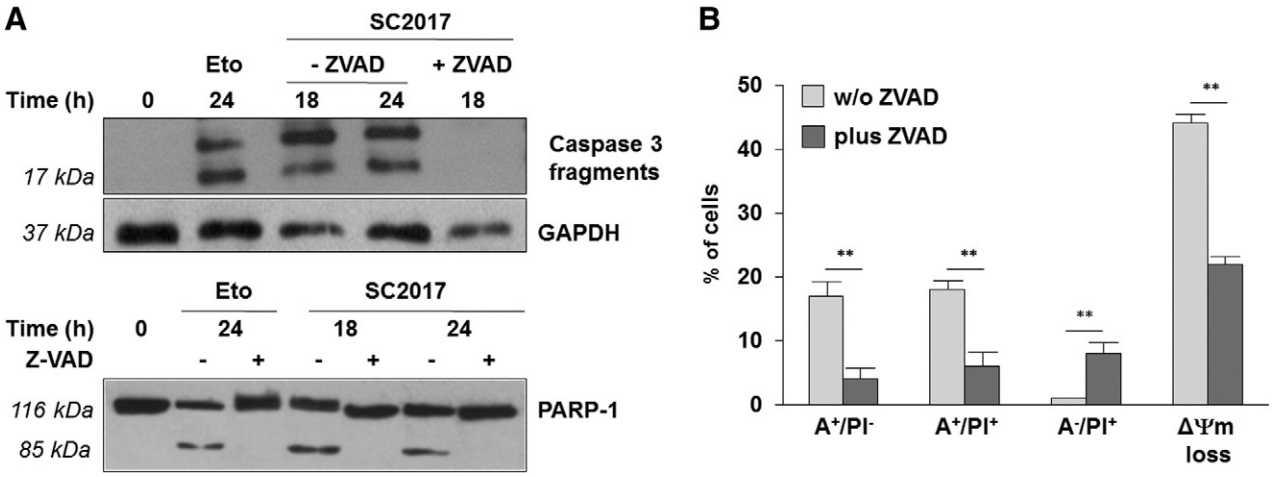


**Fig. 5.** SC2017 induces caspase-dependent apoptosis. (A) Jurkat cells were treated for the indicated times with 2.5 μM SC2017 and cell extracts were checked for the presence of caspase 3 proteolytic fragments and PARP-1 cleavage giving the 85 kDa fragment; cells receiving 10 μM etoposide (Eto) or pre-treated ZVAD before incubation with SC2017 were included as controls. The blots are representative of three. (B) Effect of ZVAD on the extent of apoptosis (see Fig. 3 for abbreviations) and ΔΨm loss in Jurkat cells exposed for 24 h to 2.5 μM SC2017. Data from samples with and without (w/o) ZVAD have been subtracted for the corresponding values in control cells. Data reported are mean values ± SEM from at least two experiments done in duplicate (**$p < 0.001$).

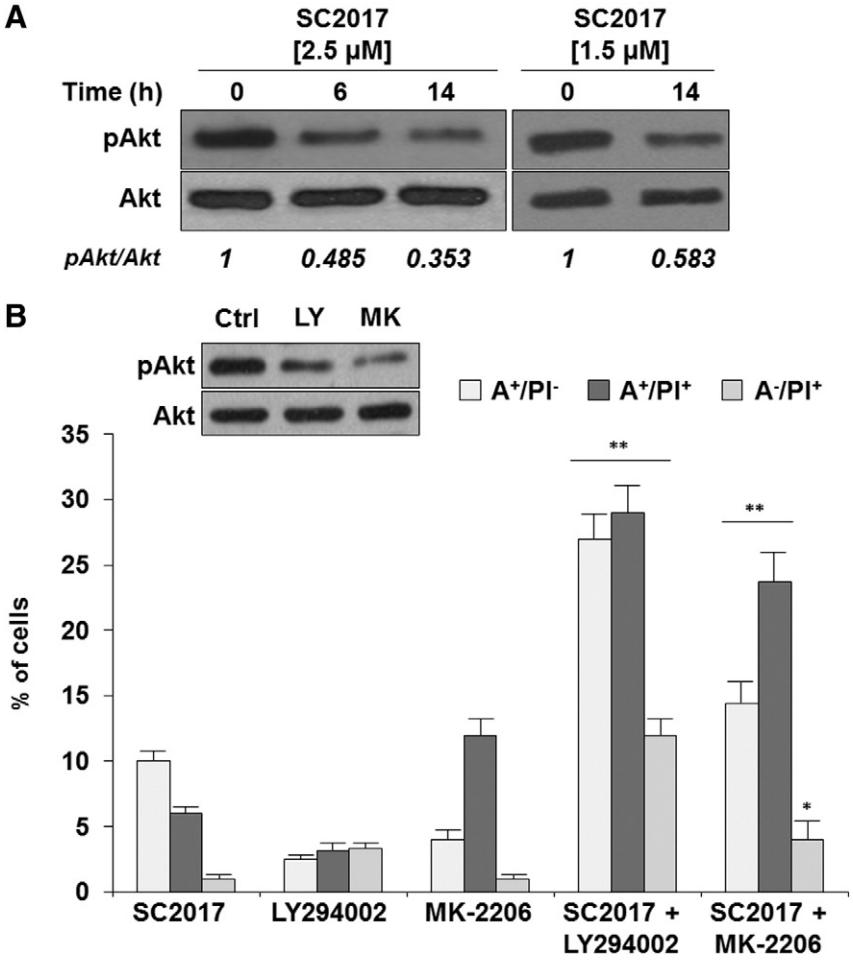


**Fig. 6.** Involvement of PI3K/Akt pathways in SC2017-induced apoptosis. (A) Jurkat cells were exposed for the indicated times to SC2017 and whole cell lysates were checked for the levels of Akt and its phosphorylated form (pAkt). Densitometry of bands is indicated: pAkt/Akt is the ratio of phosphorylated Akt to total Akt normalized to the control (time 0). The blots are representative of three. (B) Jurkat cells were incubated for 24 h with 1.5 μM SC2017 ± LY294002 (15 μM) or MK-2206 (1 μM) and then the percentages of Annexin V positive cells (see legend of Fig. 3 for abbreviations) were evaluated by flow cytometry. Data reported have been subtracted for the percentages of control cells in the corresponding gated regions (vehicle only: ≤2.2% in all quadrants; *$p < 0.05$, **$p < 0.001$ *vs* SC2017 without inhibitors. The inset represents the relative level of total and phosphorylated Akt in whole cell lysates obtained from untreated cells (Ctrl) and cells treated for 8 h with 15 μM LY294002 (LY) and 1 μM MK-2206 (MK).

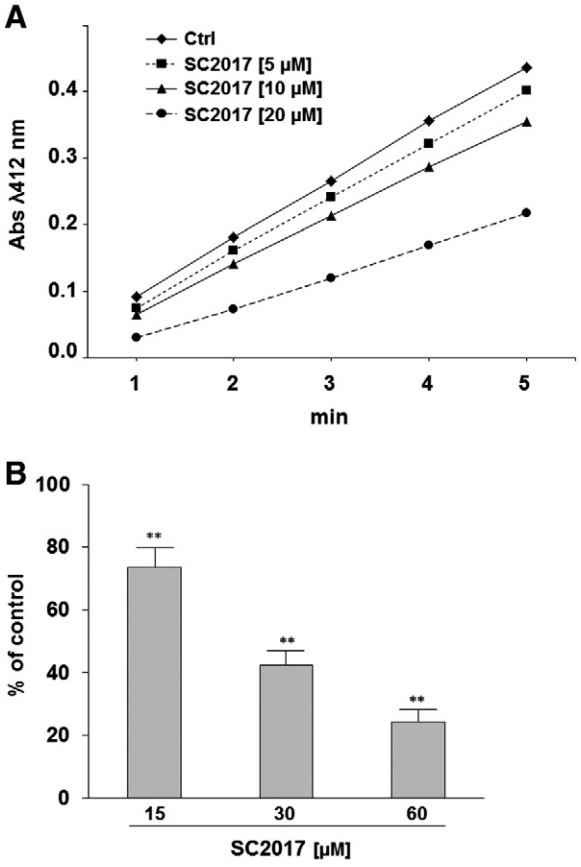


**Fig. 7.** SC2017 inhibits thioredoxin reductase activity. TrxR activity was measured using DTNB as substrate and NADPH as an electron donor. (A) Inhibition of TrxR activity by SC2017 in a cell-free system. Curves are from a single experiment representative of three with comparable results. (B) Cells were incubated with SC2017 or vehicle only for 90 min and TrxR activity was measured in whole lysates (details in Section 2.7). Data are expressed as percentage of control samples and are the mean values ± SEM from at least two experiments done in duplicate (**$p < 0.001$).

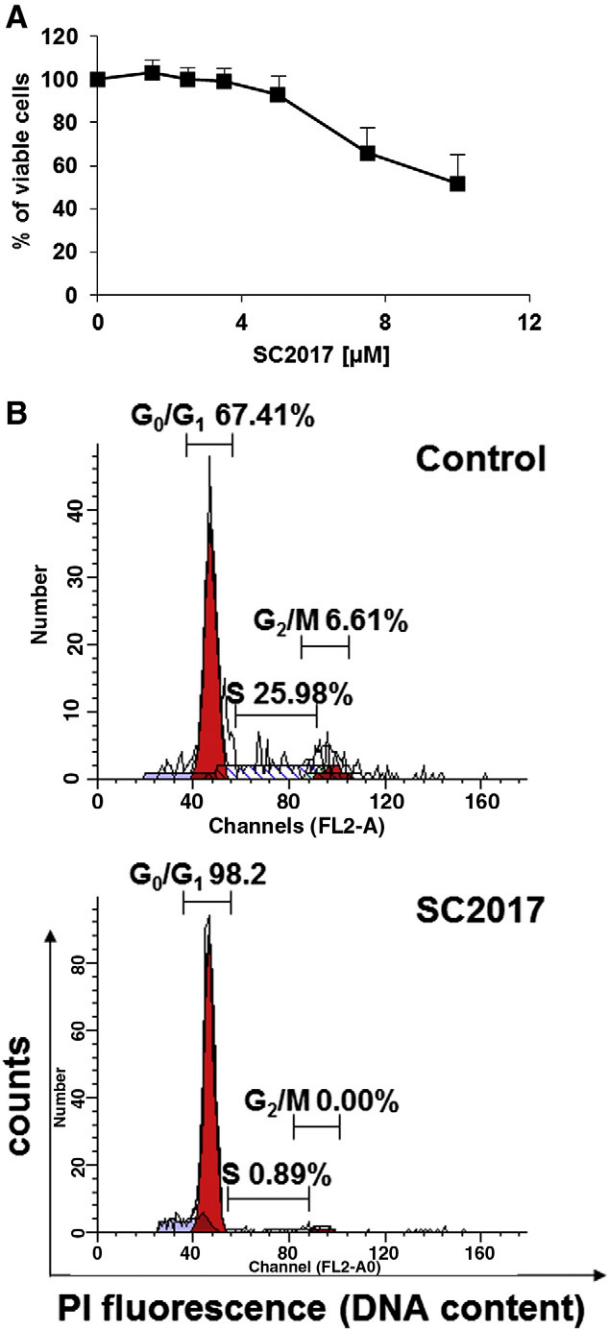


**Fig. 8.** Effect of SC2017 on resting and proliferating PBMC. (A) Freshly isolated non-proliferating PBMC were incubated with increasing doses of SC2017 or vehicle only and after 24 h incubation the number of viable cells was evaluated by MTT assay. Data are the mean values ± SEM from three experiments done in duplicate. (B) Representative histograms of DNA content in PHA-stimulated PBMC incubated with 5 μM SC2017 or vehicle only up to 72 h. Experiments were conducted in duplicate on three different PBMC preparations obtaining comparable results.

### *3.8. SC2017 inhibits xenograft tumor growth*

We evaluated the *in vivo* anti-tumor potential of SC2017 in mice bearing HCT 116 xenografts. After seven days from subcutaneous injection of HCT 116, treatments with daily delivery of SC2017 at 10 mg/kg, and as control with the same volume (100 μl) of vehicle, were performed. An evident inhibition of tumor growth was already detectable after seven days of treatment compared to vehicle (expressed as $mm^3$ ± SEM: 480.46 ± 51.62 *vs* 748.83 ± 65.66, −35.8%, $p = 0.0172$). After additional seven days of treatment, the inhibition exerted by SC2017 remained constant (1026.80 ± 81.69 *vs* 1526.62 ± 105.48, −35.7%, $p = 0.0031$) (Fig. 9). No evident sign of toxicity was revealed during the treatment, as confirmed also by any difference between the average of mice weight of the two experimental groups (SC2017: 27.13 g; vehicle: 27.50 g).

## 4. Discussion

The cytotoxic potential of SC2017, a semi-synthetic compound derived from the plant metabolite atractyligenin, has previously been demonstrated in several solid-tumor cell lines [13]. In the present study, we show that SC2017 possesses a still higher cell growth-inhibiting potential in leukemia-derived cell lines. SC2017 revealed to be a very interesting compound since its IC50 values at 24 h in Jurkat and U937 cells (1.68 and 3.2 μM, respectively) were about 3-fold lower than those of its parent compound oridonin. Notably, SC2017 displayed low cell-killing potency against normal cells, with its IC50 value in PBMC being about 5 fold higher than in Jurkat cells.

The primary response of Jurkat cells to SC2017 treatment was a delay of cell cycle progression mainly characterized by an arrest in $G_2$/M followed by cell death of blocked cells. Cyclin B1/Cdc2 complex is essential to trigger $G_2$/M phase transition [30] and cyclin B1 binding to Cdc2 promotes the phosphorylation of the kinase on Thr161, the activating site [31]. Both the levels of cyclin B1 and pCdc2 (Thr161) were reduced in SC2017-treated Jurkat cells, thus indicating cells accumulated in $G_2$ before entering in M phase.

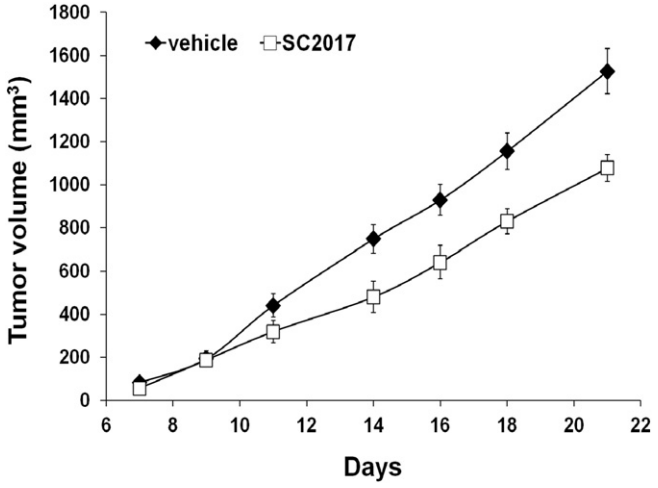


**Fig. 9.** SR inhibits xenograft tumor growth. HCT 116 xenograft tumor volume was measured three times a week. Data represent the mean values ± SEM, *p = 0.0172, **p = 0.0031 *vs* vehicle.

The presence, particularly marked at 2.5 μM SC2017, of apoptosis hallmarks, such as hypodiploidia, PS exposure on plasma membrane, and chromatin condensation indicated the chemical induced Jurkat cell death by apoptosis. Mitochondria play a central role in the SC2017-triggered apoptotic process as suggested by the early onset of electrochemical gradient dissipation and cytochrome *c* release. When released, cytochrome *c* act as cofactors for the apoptosome, thus promoting the proteolytic activation of caspase 9 and of the executor caspase 3 [21]. Accordingly, cleavage of caspase 3 and of its substrate PARP-1 was observed in SC2017-treated cells. Notably, ZVAD, a pan caspase inhibitor, prevented mitochondria depolarization less efficiently than PS exposure, thus suggesting that caspase-pathway activation occurs mainly downstream mitochondria.

Outer mitochondrial membrane permeabilization is controlled by the Bcl-2 protein family, which includes either anti- or pro-apoptotic members [22]. Since SC2017 was found not to affect the levels of the anti-apoptotic Bcl-2 member of this family, we focused on other proteins involved in the control of mitochondrial membrane permeability and cytochrome *c* release, possibly targeted by SC2017.

PI3K/Akt pathway is one of the major cell survival pathways regulating cellular proliferation, transcription, and metabolism [14]. It is known that PI3K promotes Akt activation through an initial phosphorylation at Thr308 by phosphoinositide-dependent kinase 1 (PDK1) and an additional phosphorylation at Ser473 by the mammalian target of rapamycin complex 2 (mTORC2) [32,33]. DNA-PK and several other kinases have been also shown to phosphorylate Akt at Ser473 [34]. The key role of Akt as component of the anti-apoptotic machinery is signified by its constitutive activation (phosphorylation at Ser473) in several human cancers, including leukemia [16,35,36]. Activated Akt has been shown to directly control the mitochondrial membrane and to prevent cytochrome *c* release [24,25]. Akt-dependent phosphorylation of BAD, a pro-apoptotic member of Bcl-2 family, creates binding sites for 14-3-3 scaffold proteins, which sequestrates BAD in the cytoplasm [37,38]. Consequently, BAD translocation on mitochondrial membrane to form an inactive complex with the anti-apoptotic members Bcl-xL and Bcl-2 is inhibited. Akt has been shown to prevent cells to undergo apoptotic death also by inhibiting caspase 9 and caspase 3 [39]. We found that SC2017 treatment caused a marked and dose-dependent decrease of constitutive Akt phosphorylation at Ser473. The involvement of PI3K/Akt in SC2017-induced apoptosis was further confirmed by the increase of apoptotic death observed when a combined treatment of SC2017 with PI3K/Akt pathway inhibitors was used. Interestingly, the percentage of PS exposing cells and $\Delta\Psi m$ loss was more markedly increased in the presence of LY294002, an inhibitor of PI3K, than in the presence of MK-2206, an allosteric inhibitor of Akt. The more than additive effect of LY294002 is not completely surprising because LY294002 is known to inhibit several other kinases and in particular casein kinase 2 (Ck2) [40]. Ck2, a pleiotropic member of the protein kinase superfamily [41], is known to prevent apoptosis, promote cell proliferation, and be highly expressed in cancers [42]. Notably, Di Maira et al. showed that CK2 phosphorylates and up-regulates Akt in Jurkat cells [43].

At least, we could speculate that the inhibition of Akt activation is one of the mechanisms underlying SC2017 induced G2 arrest. PI3K has, indeed, been shown to promote cell entering mitosis through Akt-dependent regulation of CdK1 (Cdc2) inhibitors/activators and of the level of the cyclin-dependent kinase inhibitor, $p21^{Cip1}$ [44].

The Trx system, comprising NADPH, Trx and TrxR, beyond its intrinsic antioxidant activity, has been shown to be a signaling intermediate [15,17]. Trx controls nuclear translocation and/or activity of several transcription factors and prevents apoptosis. Trx protects mitochondria from permeability transition pore (PTP) opening and cytochrome *c* release and inhibits the activation of apoptosis signal-regulating kinase 1 (ASK1). TrxR catalytic thiols and/or the exposed selenocysteine [28,29] are good Michael acceptors for the α,β-unsaturated carbonyl group present in the SC2017 structure [10]. Accordingly, the ability of SC2017 to inhibit TrxR activity was observed both in a cell-free system and in Jurkat cells. The reactivity of the electrophilic group towards TrxR Cys/Sec is supported by the recent findings on the Trx inhibitory activity of oridonin [45]. However, differently from oridonin [46,47], the inhibitory effect of SC2017 seemed more specific because it is not dependent upon a generalized ROS elevation (redox catastrophe).

Finally, we conducted xenograft tumor experiments to assess SC2017 anti-tumor potential also *in vivo*. SC2017 significantly decreased tumor growth of HCT 116 xenografts. This result seems encouraging both in terms of tumor growth inhibition and in terms of toxicity. By considering the lower susceptibility of HCT 116 cells with respect to Jurkat and U937 cells, we could speculate that the *in vivo* effectiveness of SC2017 might be higher using human leukemia cells' xenograft model in mice.

In conclusion, the present study highlights the tumor cell-specific growth inhibition activity of the semi-synthetic *ent*-kaurane SC2017 *in vitro* and *in vivo* models. In addition, the inhibitory effect of SC2017 on PI3K/Akt pathway and the Trx system, two key components of tumor cell survival machinery, has been demonstrated. Since constitutive activation of Akt and the high levels of Trx and/or TrxR have been reported in many different human malignancies [16,17], chemicals targeting PI3K/Akt signaling pathway and the Trx system have been proposed as chemotherapeutics [48,49]. On this basis, our data suggest that SC2017 could be considered a promising candidate, alone or in combination, for cancer therapy.

Supplementary data to this article can be found online at http://dx.doi.org/10.1016/j.bbagen.2013.11.023.

## Acknowledgements

This work was supported by an Internal Grant of the University of Salerno, Italy.

## References

[1] J.R. Hanson, Diterpenoids, Nat. Prod. Rep. 26 (2009) 1156–1171.
[2] H.D. Sun, S.X. Huang, Q.B. Han, Diterpenoids from Isodon species and their biological activities, Nat. Prod. Rep. 23 (2006) 673–698.
[3] P.A. Garcia, A.B. de Oliveira, R. Batista, Occurrence, biological activities and synthesis of kaurane diterpenes and their glycosides, Molecules 12 (2007) 455–483.
[4] L. Wang, D. Li, C. Wang, Y. Zhang, J. Xu, Recent progress in the development of natural *ent*-kaurane diterpenoids with anti-tumour activity, Mini-Rev. Med. Chem. 11 (2011) 910–919.
[5] Y. Ruiz, J. Rodriguez, F. Arvelo, A. Usubillaga, M. Monsalve, N. Diez, I. Galindo-Castro, Cytotoxic and apoptosis-inducing effect of *ent*-15-oxo-kaur-16-en-19-oic acid, a derivative of grandiflorolic acid from *Espeletia schultzii*, Phytochemistry 69 (2008) 432–438.

[6] P.C. Kuo, Y.C. Shen, M.L. Yang, S.H. Wang, T.D. Thang, N.X. Dung, P.C. Chiang, K.H. Lee, E.J. Lee, T.S. Wu, Crotonkinins A and B and related diterpenoids from *Croton tonkinensis* as anti-inflammatory and antitumour agents, J. Nat. Prod. 70 (2007) 1906–1909.
[7] X.T. Liu, Y. Shi, B. Yu, I.D. Williams, H.H.Y. Sung, Q. Zhang, J.Y. Liang, N.Y. Ip, Z.D. Min, Antibacterial diterpenoids from *Sagittaria pygmea*, Planta Med. 73 (2007) 84–90.
[8] M. Bruno, S. Rosselli, I. Pibiri, N. Kilgore, K.H. Lee, Anti-HIV agents derived from the *ent*-kaurane diterpenoids linearol, J. Nat. Prod. 65 (2002) 1594–1597.
[9] C. Avonto, O. Taglialatela-Scafati, F. Pollastro, A. Minassi, V. Di Marzo, L. De Petrocellis, G. Appendino, An NMR spectroscopic method to identify and classify thiol-trapping agents: revival of Michael acceptors for drug discovery? Angew. Chem. Int. Ed. Engl. 50 (2011) 467–471.
[10] F. Dal Piaz, P. Nigro, A. Braca, N. De Tommasi, M.A. Belisario, 13-Hydroxy-15-oxo-zoapatlin, an *ent*-kaurane diterpene, induces apoptosis in human leukemia cells, affecting thiol-mediated redox regulation, Free Radic. Biol. Med. 43 (2007) 1409–1422.
[11] W. Tan, J. Lu, M. Huang, Y. Li, M. Chen, G. Wu, J. Gong, Z. Zhong, Z. Xu, Y. Dang, J. Guo, X. Chen, Y. Wang, Anti-cancer natural products isolated from Chinese medicinal herbs, Chin. Med. 6 (2011) 27–41.
[12] Z. Liu, L. Ouyang, H. Peng, Z.W. Zhang, Oridonin: targeting programmed cell death pathways as an anti-tumour agent, Cell Prolif. 45 (2012) 499–507.
[13] S. Rosselli, M. Bruno, A. Maggio, G. Bellone, T.H. Chen, K.F. Bastow, K.H. Lee, Cytotoxic activity of some natural and synthetic kauranes, J. Nat. Prod. 70 (2007) 347–352.
[14] B. Vanhaesebroeck, L. Stephens, P. Hawkins, PI3K signalling: the path to discovery and understanding, Nat. Rev. Mol. Cell Biol. 13 (2012) 195–203.
[15] J. Lu, A. Holmgren, Thioredoxin system in cell death progression, Antioxid. Redox Signal. 17 (2012) 1738–1747.
[16] I. Hers, E.E. Vincent, J.M. Tavaré, Akt signalling in health and disease, Cell. Signal. 23 (2011) 1515–1527.
[17] E.S. Arnér, A. Holmgren, The thioredoxin system in cancer, Semin. Cancer Biol. 16 (2006) 420–426.
[18] R. Cotugno, R. Fortunato, A. Santoro, D. Gallotta, A. Braca, N. De Tommasi, M.A. Belisario, Effect of the sesquiterpene lactone coronopilin on leukemia cell growth: cell type-specific induction of apoptosis and mitotic catastrophe, Cell Prolif. 45 (2012) 53–65.
[19] D. Gallotta, P. Nigro, R. Cotugno, P. Gazzerro, M. Bifulco, M.A. Belisario, Rimonabant-induced apoptosis in leukemia cell lines: activation of caspase-dependent and -independent pathways, Biochem. Pharmacol. 80 (2010) 370–380.
[20] X. Huang, H.D. Halicka, F. Traganos, T. Tanaka, A. Kurose, Z. Darzynkiewicz, Cytometric assessment of DNA damage in relation to cell cycle phase and apoptosis, Cell Prolif. 38 (2005) 223–243.
[21] A. Jourdain, J.C. Martinou, Mitochondrial outer-membrane permeabilization and remodelling in apoptosis, Int. J. Biochem. Cell Biol. 41 (2009) 1884–1889.
[22] J. Lindsay, M.D. Esposti, A.P. Gilmore, Bcl-2 proteins and mitochondria-specificity in membrane targeting for death, Biochim. Biophys. Acta 1813 (2011) 532–539.
[23] J. Park, J. Lee, C. Choi, Mitochondrial network determines intracellular ROS dynamics and sensitivity to oxidative stress through switching inter-mitochondrial messengers, PLoS One 6 (2011) e23211.
[24] S.G. Kennedy, E.S. Kandel, T.K. Cross, N. Hay, Akt/Protein kinase B inhibits cell death by preventing the release of cytochrome *c* from mitochondria, Mol. Cell. Biol. 19 (1999) 5800–5810.
[25] Y. Kanamaru, S. Sekine, H. Ichijo, K. Takeda, The phosphorylation-dependent regulation of mitochondrial proteins in stress responses, J. Signal Transduct. 2012 (2012)[ID 931215].
[26] C.C. Su, Y.P. Lin, Y.J. Cheng, J.Y. Huang, W.J. Chuang, Y.S. Shan, B.C. Yang, Phosphatidylinositol 3-kinase/Akt activation by integrin-tumor matrix interaction suppresses Fas-mediated apoptosis in T cells, J. Immunol. 179 (2007) 4589–4597.
[27] D. Bressanin, C. Evangelisti, F. Ricci, G. Tabellini, F. Chiarini, P.L. Tazzari, F. Buontempo, P. Pagliaro, A. Pession, J.A. McCubrey, A.M. Martelli, Harnessing the PI3K/Akt/mTOR pathway in T-cell acute lymphoblastic leukemia: eliminating activity by targeting at different levels, Oncotarget 3 (2012) 811–823.
[28] D. Mustacich, G. Powis, Thioredoxin reductase, Biochem. J. 346 (2000) 1–8.
[29] T. Sandalova, L. Zhong, Y. Lindqvist, A. Holmgren, G. Schneider, Three-dimensional structure of a mammalian thioredoxin reductase: implications for mechanism and evolution of a selenocysteine-dependent enzyme, Proc. Natl. Acad. Sci. U. S. A. 98 (2001) 9533–9538.
[30] P. Nurse, Universal control mechanism regulating onset of M-phase, Nature 344 (1990) 503–508.
[31] G. Draetta, Cdc2 activation: the interplay of cyclin binding and Thr161 phosphorylation, Trends Cell Biol. 3 (1993) 287–289.
[32] L. Stephens, K. Anderson, D. Stokoe, H. Erdjument-Bromage, G.F. Painter, A.B. Holmes, P.R. Gaffney, C.B. Reese, F. McCormick, P. Tempst, J. Coadwell, P.T. Hawkins, Protein kinase B kinases that mediate phosphatidylinositol 3,4,5 trisphosphate dependent activation of protein kinase B, Science 279 (1998) 710–714.
[33] D.D. Sarbassov, D.A. Guertin, S.M. Ali, D.M. Sabatini, Phosphorylation and regulation of Akt/PKB by the rictor–mTOR complex, Science 307 (2005) 1098–1101.
[34] E. Fayard, L.A. Tintignac, A. Baudry, B.A. Hemmings, Protein kinase B/Akt at a glance, J. Cell Sci. 118 (2005) 5675–5678.
[35] T.L. Yuan, L.C. Cantley, PI3K pathway alterations in cancer: variations on a theme, Oncogene 27 (2008) 5497–5510.
[36] J. Zhuang, S.F. Hawkins, M.A. Glenn, K. Lin, G.G. Johnson, A. Carter, J.C. Cawley, A.R. Pettitt, Akt is activated in chronic lymphocytic leukemia cells and delivers a pro-survival signal: the therapeutic potential of Akt inhibition, Haematologica 95 (2010) 110–118.
[37] S.R. Datta, H. Dudek, X. Tao, S. Masters, H. Fu, Y. Gotoh, M.E. Greenberg, Akt phosphorylation of BAD couples survival signal to the cell-intrinsic death machinery, Cell 91 (1997) 231–241.
[38] J.P. Zha, H. Harada, E. Yang, J. Jockel, S.J. Korsmeyer, Serine phosphorylation of death agonist Bad in response to survival factor results in binding to 14-3-3 not Bcl-X(L), Cell 87 (1996) 619–628.
[39] H. Zhou, X.M. Li, J. Meinkoth, R.N. Pittman, Akt regulates cell survival and apoptosis at a post-mitochondrial level, J. Cell Biol. 151 (2000) 483–494.
[40] S.P. Davies, H. Reddy, M. Caivano, P. Cohen, Specificity and mechanism of action of some commonly used protein kinase inhibitors, Biochem. J. 351 (2000) 95–105.
[41] F. Meggio, L.A. Pinna, One-thousand-and-one substrates of protein kinase CK2? FASEB J. 17 (2003) 349–368.
[42] J.H. Trembley, Z. Chen, G. Unger, J. Slaton, B.T. Kren, C. Van Waes, K. Ahmed, Emergence of protein kinase CK2 as a key target in cancer therapy, Biofactors 36 (2010) 187–195.
[43] G. Di Maira, M. Salvi, G. Arrigoni, O. Marin, S. Sarno, F. Brustolon, L.A. Pinna, M. Ruzzene, Protein kinase CK2 phosphorylates and upregulates Akt/PKB, Cell Death Differ. 12 (2005) 668–677.
[44] N. Xu, Y. Lao, Y. Zhang, D.A. Gillespie, Akt: a double-edged sword in cell proliferation and genome stability, J. Oncol. 2012 (2012)[ID 951724].
[45] T. Zhen, C.F. Wu, P. Liu, H.Y. Wu, G.B. Zhou, Y. Lu, J.X. Liu, Y. Liang, K.K. Li, Y.Y. Wang, Y.Y. Xie, M.M. He, H.M. Cao, W.N. Zhang, L.M. Chen, K. Petrie, S.J. Chen, Z. Chen, Targeting of AML1-ETO in t(8;21) leukemia by oridonin generates a tumor suppressor-like protein, Sci. Transl. Med. 4 (2012) 127ra38.
[46] Y. Cheng, F. Qiu, Y.C. Ye, Z.M. Guo, S. Tashiro, S. Onodera, T. Ikejima, Autophagy inhibits reactive oxygen species-mediated apoptosis via activating p38-nuclear factor-kappa B survival pathways in oridonin-treated murine fibrosarcoma L929 cells, FEBS J. 276 (2009) 1291–1306.
[47] F.H. Gao, F. Liu, W. Wei, L.B. Liu, M.H. Xu, Z.Y. Guo, W. Li, B. Jiang, Y.L. Wu, Oridonin induces apoptosis and senescence by increasing hydrogen peroxide and glutathione depletion in colorectal cancer cells, Int. J. Mol. Med. 29 (2012) 649–655.
[48] K.D. Courtney, R.B. Corcoran, J.A. Engelman, The PI3K pathway as drug target in human cancer, J. Clin. Oncol. 28 (2010) 1075–1083.
[49] D.F. Mahmood, A. Abderrazak, E.H. Khadija, T. Simmet, M. Rouis, The thioredoxin system as a therapeutic target in human health and disease, Antioxid. Redox Signal. 19 (2013) 1266–1303.